Impulse Functions Applied to Compute Pressure Change During Injectivity Tests

Renan Vieira Bela[a,*], Sinesio Pesco[a], Abelardo Barreto Jr.[a]

[a]*PUC-Rio, Departamento de Matemática*

Abstract

This work presents a solution to compute pressure change during injectivity tests in single-layer reservoirs with vertical wells using impulse functions (or Green's functions). The proposed formulation employs a radially composite reservoir approach to depict the waterfront propagation and assumes a piston-like fluid displacement. Then, pressure change in multilayer commingled reservoirs may be obtained by combining the single-layer solution for each layer. Layer properties such as permeability, thickness and porosity may be different in each layer. The presented single-layer solution is also combined with Newmann's product to derive an approximate formulation for pressure change in single-layer reservoirs with horizontal wells. Pressure and layer flow-rate profiles computed using the proposed formulation showed a good agreement when compared to previously existing solutions and a commercial flow simulator. Moreover, this work also estimates layer individual permeabilities from pressure and layer flow-rate data.

Keywords: Injectivity Tests, Pressure Transient Analysis, Green's Functions, Reservoir Characterization

1. Introduction

Pressure transient analysis is crucial in reservoir engineering, as it provides valuable estimates about reservoir features and parameters.

Typically, well testing is performed to estimate reservoir properties (Lefkovits et al., 1961, Raghavan, 1989, Ahmed, 2010). Alternatively, parameters such as permeability and outer boundary condition may be estimated based on data collected during an injectivity test (Banerjee et al., 1998, Peres et al., 2006).

Injectivity tests have gained more attention recently, as they are operationally safer and avoid dealing with fluid disposal or flaring - hence, presenting lower environmental impact than conventional well testing (Borello et al., 2019, Bonafé et al., 2020). The reduced carbon footprint compared to conventional well testing becomes particularly important considering that many oil field companies committed to substantially decrease greenhouse gas emissions in a foreseeable future (Petrobras, 2021, Occidental, 2021, Petronas, 2021, Lukoil, 2021, Equinor, 2021, Shell, 2021).

Pressure transient data may be easily interpreted using analytical solutions that accurately describe pressure behavior in the reservoir. Additionally, analytical models are effortlessly coupled with nonlinear regression techniques and optimization methods (Coutinho et al., 2010, Silva et al., 2021, Bela et al., 2022).

Thompson and Reynolds (1997) developed a

*Corresponding author

Email addresses: renanvb1@mat.puc-rio.br (Renan Vieira Bela), sinesio@puc-rio.br (Sinesio Pesco), abelardo.puc@gmail.com (Abelardo Barreto Jr.)

solution for single-layered radially heterogeneous reservoirs. Their model has inspired the development of analytical solutions for pressure change during injectivity tests (Banerjee et al., 1998, Peres and Reynolds, 2003, Peres et al., 2006, Boughara and Reynolds, 2009, Bonafé et al., 2020).

Banerjee et al. (1998) presented a formulation for injection/falloff tests in single-layer reservoirs with vertical wells. As outlined by Banerjee et al. (1998), their model assume that the rate-transient pulse propagates faster than the flood front. Hence, flow-rate inside the flooded region remains constant during the injection period, as illustrated in Fig. 1.

Peres and Reynolds (2003) established objective criteria to verify that, in single-layer reservoirs, such condition holds for most cases of practical interest and also proposed a solution for injectivity tests in single-layer reservoirs with horizontal wells.

Boughara and Reynolds (2009) included the thermal effects into the formulation and applied a non-linear regression method to estimate reservoir properties. Bonafé et al. (2020) provided an approximate model for injectivity tests in single-layer reservoirs considering a multiple flow-rate scheme.

Analytical solutions for injectivity tests in multilayer reservoirs (Barreto Jr. et al., 2011, Bela et al., 2019, 2020b) were inspired by the single-layer solutions (Banerjee et al., 1998, Peres and Reynolds, 2003, Peres et al., 2006, Boughara and Reynolds, 2009, Bonafé et al., 2020) and, hence, by the Thompson and Reynolds (1997) steady-state theory. However, in multilayer reservoirs, layer flow-rates at the wellbore may change in time due to differences between layer properties (Gao, 1987, Ehlig-Economides and Joseph, 1987, Bela et al., 2020a, Silva et al., 2021).

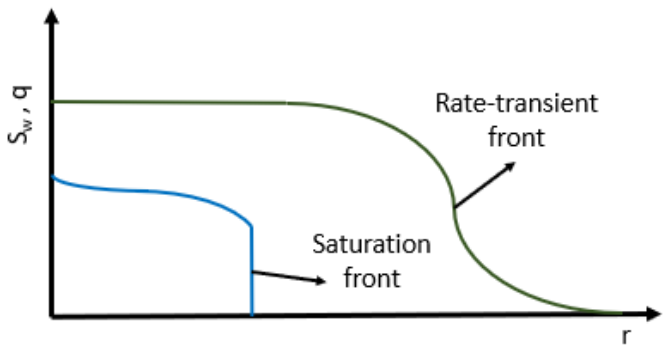

Figure 1: Schematics of rate transient front and water saturation front in a single-layer reservoir

Fig. 2 exhibits an illustrative representation of layer flow-rate profiles at the wellbore and the respective rate transient fronts in a two-layered reservoir. As may be observed in Fig. 2, it is not possible to assure that flow-rate is constant throughout the flooded region in multilayer systems, due to the rate transient that occurs at the wellbore. Therefore, in a strict sense, the Thompson and Reynolds (1997) steady-state theory does not hold for multilayer formations.

Neto et al. (2020) proposed an alternative solution for injectivity tests in single-layer reservoirs. The flooded zone and the uninvaded region are described using a radially composite reservoir approach, where the interface between regions (that is, the water front radius) moves in time (Bratvold and Horne, 1990). The formulation presented by Neto et al. (2020) does not require flow-rate within the flooded region to be constant. On the other hand, it assumes a piston-like fluid displacement.

Mastbaum et al. (2021) also employed a radially heterogeneous reservoir model to develop a solution for multilayer stratified reservoirs, while Viana (2021) included formation crossflow effects into the solution.

Green's functions (or impulse functions) for single-phase flow of slightly compressible fluids in single-layer reservoirs are known (Gringarten and Ramey Jr., 1973, Chen et al., 1991). Kuchuk and Wilkinson (1991) developed an algorithm to determine the pressure response in commingled reservoirs using the appropriate single-layer impulse function for each layer. This algorithm was endorsed by Spath et al. (1994), in a work that also detailed how layer flow-rates at the wellbore may

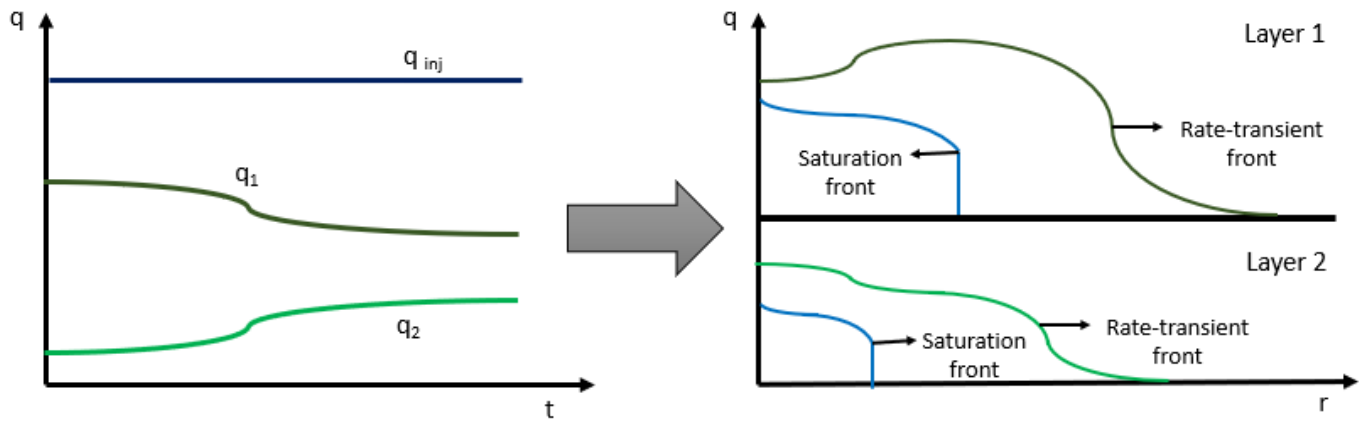

Figure 2: Layer flow-rate profiles at the wellbore (on the left) and rate and saturation fronts in each layer

be computed. Lu et al. (2019) applied Green's functions to develop a formulation for well tests in two-layer reservoirs with formation crossflow. However, to the best of our knowledge, impulse functions have not yet been applied to evaluate the pressure change in reservoirs under two-phase flow.

Therefore, the first goal of this work is to apply Green's functions to determine the pressure change during injectivity tests in single-layer reservoirs using a radially composite approach. Then, the single-layer solution is coupled to the algorithm presented by Kuchuk and Wilkinson (1991) and Spath et al. (1994) to obtain pressure and flow-rate profiles in multilayer reservoirs. Additionally, an approximate solution for pressure change during injectivity tests in single-layer reservoirs with horizontal wells is derived by applying Newman (1936) product and the presented single-layer formulation.

The proposed models were validated via comparison, for a set of synthetic cases, to a commercial finite difference-based flow simulator and to the previously existing solutions (Peres and Reynolds, 2003, Barreto Jr. et al., 2011, Mastbaum et al., 2021). Furthermore, the Delta Transient Method (Galvão and Guimarães, 2017, Guimarães and Galvão, 2017) was applied to estimate layer permeabilities in the multilayer cases.

2. Proposed Formulation

This Section outlines the proposed formulation for injectivity tests in single-layer reservoirs with vertical wells using impulse functions. This formulation may be coupled to the algorithm introduced by Kuchuk and Wilkinson (1991) to evaluate the pressure behavior in multilayer reservoirs with vertical wells. Besides, an approximate model for injectivity tests in single-layer reservoirs with horizontal wells is obtained, combining the proposed model for radially composite reservoirs with an unorthodox application of Newman (1936) product.

The reservoir is assumed to be homogeneous, laterally infinite and initially in equilibrium. Fluids are considered to be slightly compressible, with constant viscosity and compressibility. The presented formulation considers that capillary and gravitational forces are negligible. An isothermal flow is considered and a piston-like fluid displacement is assumed. Finally, all computations are made assuming a consistent set of units.

2.1. Impulse Function for Single-Layer Reservoirs with Vertical Wells

Using a radially composite approach, water injection in a single-layer reservoir may be understood as a problem of a radially heterogeneous reservoir with a moving boundary $r_F(t)$ (Bratvold

and Horne, 1990, Mastbaum et al., 2021). Formation damage is included into the model by defining an annular region, concentric to the wellbore axis, where the permeability k_s is different than the reservoir permeability k (Neto, 2019, Neto et al., 2020). Wellbore storage will be initially neglected and incorporated into the model afterwards.

Figs. 3 to 6 show the reservoir top and lateral view at two distinct stages: while the water front is within the damaged region (Figs. 3 and 4) and after the flooded region has overcome the skin radius (Figs. 5 and 6). In Figs. 3 to 6, the skin radius is represented as r_s, while r_w denotes the wellbore radius, r_F denotes the water front radius and r_e denotes the reservoir outer radius.

The water front radius at each time step is determined as (Buckley and Leverett, 1942):

$$r_F(t) = \sqrt{r_w^2 + \frac{\int_0^t q(\tau)d\tau}{\pi\phi h} f'_w(S_w)}, \qquad (1)$$

where q represents the injection flow-rate, ϕ denotes the reservoir porosity, h indicates the formation thickness and $f'_w(S_w)$ stands for the fractional flow derivative. For a piston-like fluid displacement, f'_w is computed as (Neto et al., 2020, Viana, 2021, Mastbaum et al., 2021):

$$f'_w(S_w) = \frac{1}{1 - S_{wi} - S_{or}}, \qquad (2)$$

where S_{wi} represents the water initial saturation and S_{or} denotes the oil residual saturation.

The reservoir, then, may be split into three distinct regions, depending on the flood front position. While the water front is within the damaged zone:

Reg. 1: goes from $r = r_w$ to $r = r_F(t)$

Reg. 2: goes from $r = r_F(t)$ to $r = r_s$

Reg. 3: goes from $r = r_s$ to r_e

And after the water front has overcome the skin zone:

Reg. 1: goes from $r = r_w$ to $r = r_s$

Reg. 2: goes from $r = r_s$ to $r = r_F(t)$

Reg. 3: goes from $r = r_F(t)$ to r_e

According to the model assumptions previously mentioned, flow in each region obeys the diffusivity equation (Ehlig-Economides and Joseph, 1987, Neto, 2019):

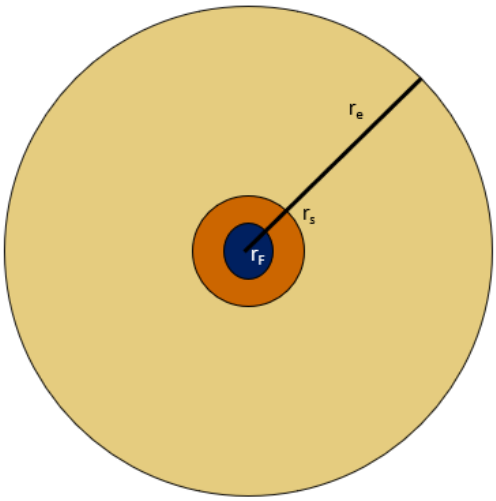

Figure 3: Reservoir top view for $r_F(t) < r_s$.

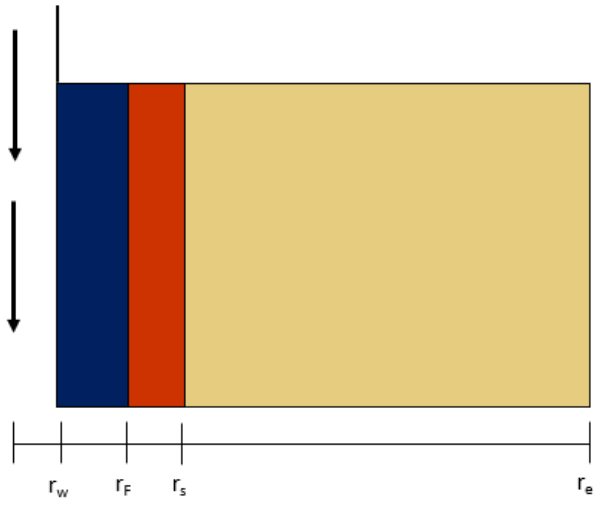

Figure 4: Reservoir lateral view for $r_F(t) < r_s$.

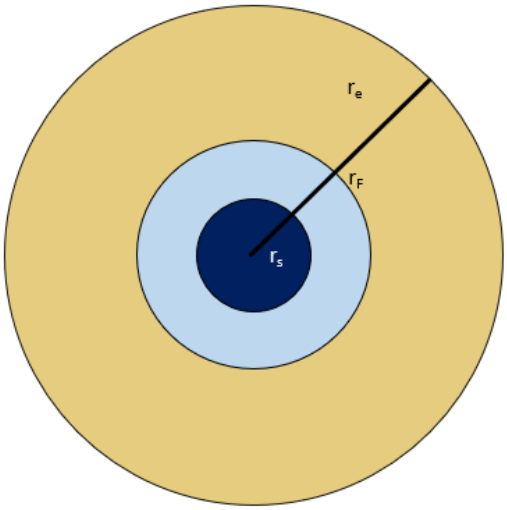

Figure 5: Reservoir top view for $r_F(t) > r_s$.

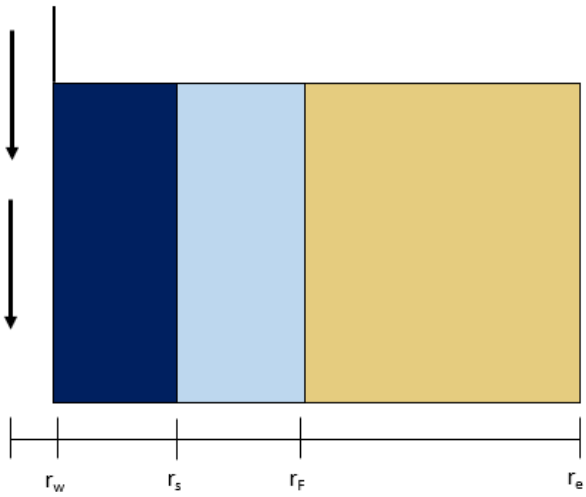

Figure 6: Reservoir lateral view for $r_F(t) > r_s$.

$$\frac{1}{r}\frac{\partial}{\partial r}\left(r\frac{\partial \Delta p_i}{\partial r}\right) - \frac{1}{\eta_i}\frac{\partial \Delta p_i}{\partial t} = 0, \tag{3}$$

where the subscript $i \in \{1, 2, 3\}$ indexes the region, r stands for the radius, t denotes the time and $\Delta p(r, t) = p(r, t) - p(r, t = 0)$ indicates the pressure change resulting from the water injection. The hydraulic diffusivity η_i is defined as (Gao, 1987, Lu et al., 2019):

$$\eta_i = \frac{k_i \lambda_i}{\phi c_t}, \tag{4}$$

where $\lambda_i = k_{ri}/\mu_i$ represents the fluid mobility (Peres and Reynolds, 2003, Barreto Jr. et al., 2011, Bela et al., 2019, Silva et al., 2021), considering the suitable fluid that flows in region i; that is, oil or water.

The initial condition, inner and outer boundary conditions for the problem are given by:

Initial Condition (IC):

$$\Delta p_i(r, t = 0) = 0. \tag{5}$$

Inner Boundary Condition (IBC):

$$\lim_{r \to r_w} 2\pi h k_1 \lambda_1 \left(r\frac{\partial \Delta p_1}{\partial r}\right) = \delta(t), \tag{6}$$

where $\delta(t)$ denotes the Dirac delta function. The IBC defined in Eq. (6) represents an instant injection of a unitary volume of water.

Outer Boundary Condition (OBC):

$$\lim_{r_e \to \infty} \Delta p_3(r = r_e, t) = 0. \tag{7}$$

Note that the problem defined by Eqs. (3) to (7) remains ill-posed so far, as the PDE presented in Eq. (3) demands two spatial conditions per region. The missing spatial conditions are obtained from pressure continuity and mass conservation at the interface between regions, yielding coupling conditions between regions (or CCRs) (Nie et al., 2011, Neto, 2019, Neto et al., 2020, Mastbaum et al., 2021, Viana, 2021):

Pressure CCR:

$$\Delta p_i(r \to r_i^-, t) = \Delta p_{i+1}(r \to r_i^+, t). \tag{8}$$

Flow-rate CCR:

$$k_i \lambda_i \left(r\frac{\partial \Delta p_i}{\partial r}\right)\bigg|_{r \to r_i^-} = k_{i+1}\lambda_{i+1} \left(r\frac{\partial \Delta p_{i+1}}{\partial r}\right)\bigg|_{r \to r_i^+}, \tag{9}$$

where $i \in \{1, 2\}$. Eqs. (8) and (9) are required to assure that pressure and flow-rate profiles along the reservoir are continuous.

Applying Laplace transform to the problem defined by Eqs. (3) to (9), the following ODE is obtained:

$$\frac{1}{r}\frac{\partial}{\partial r}\left(r\frac{\partial\overline{\Delta p}_i}{\partial r}\right) - \frac{u\overline{\Delta p}_i}{\eta_i} = 0, \tag{10}$$

for $i \in \{1, 2, 3\}$, where u denotes the Laplace variable.

The general solution of Eq. (10) is given by (Lefkovits et al., 1961, Prats et al., 2020):

$$\overline{\Delta p}_i(r, u) = a_i I_0\left(r\sqrt{\frac{u}{\eta_i}}\right) + b_i K_0\left(r\sqrt{\frac{u}{\eta_i}}\right). \tag{11}$$

Taking the derivative of Eq. (11) with respect to the radius (Abramowitz and Stegun, 1964):

$$\frac{\partial\overline{\Delta p}_i}{\partial r} = \sqrt{\frac{u}{\eta_i}}\left[a_i I_1\left(r\sqrt{\frac{u}{\eta_i}}\right) - b_i K_1\left(r\sqrt{\frac{u}{\eta_i}}\right)\right]. \tag{12}$$

Relations between the coefficients a_i and b_i in each region may be obtained from the boundary and coupling conditions. The outer boundary condition defined in Eq. (7) implies that $a_3 = 0$ (Ehlig-Economides and Joseph, 1987, Abramowitz and Stegun, 1964).

From Eqs. (6) and (12), the inner boundary condition in Laplace domain may be written as:

$$\begin{aligned} a_1 I_1\left(r_w\sqrt{\frac{u}{\eta_1}}\right) - b_1 K_1\left(r_w\sqrt{\frac{u}{\eta_1}}\right) = \\ = \frac{1}{r_w}\sqrt{\frac{\eta_1}{u}}\frac{1}{2\pi h k_1 \lambda_1}. \end{aligned} \tag{13}$$

From Eq. (11) and the CCRs defined in Eq. (8), pressure equality at the interface between regions implies that:

$$\begin{aligned} a_i I_0\left(r_i\sqrt{\frac{u}{\eta_i}}\right) + b_i K_0\left(r_i\sqrt{\frac{u}{\eta_i}}\right) - \\ - a_{i+1} I_0\left(r_i\sqrt{\frac{u}{\eta_{i+1}}}\right) - b_{i+1} K_0\left(r_i\sqrt{\frac{u}{\eta_{i+1}}}\right) = 0, \end{aligned} \tag{14}$$

for $i \in \{1, 2\}$.

Finally, from Eqs. (11) and (9), mass conservation at the interface between regions is expressed as:

$$\begin{aligned} a_i\frac{uk_i\lambda_i}{\sqrt{\eta_i}} I_1\left(r_i\sqrt{\frac{u}{\eta_i}}\right) - b_i\frac{uk_i\lambda_i}{\sqrt{\eta_i}} K_1\left(r_i\sqrt{\frac{u}{\eta_i}}\right) - \\ - a_{i+1}\frac{uk_{i+1}\lambda_{i+1}}{\sqrt{\eta_{i+1}}} I_1\left(r_i\sqrt{\frac{u}{\eta_{i+1}}}\right) + \\ + b_{i+1}\frac{uk_{i+1}\lambda_{i+1}}{\sqrt{\eta_{i+1}}} K_1\left(r_i\sqrt{\frac{u}{\eta_{i+1}}}\right) = 0, \end{aligned} \tag{15}$$

for $i \in \{1, 2\}$.

Writing Eqs. (13) to (15) as a linear system:

$$[M]\begin{bmatrix} a_1 \\ b_1 \\ a_2 \\ b_2 \\ b_3 \end{bmatrix} = \begin{bmatrix} \frac{1}{r_w}\sqrt{\frac{\eta_1}{u}}\frac{1}{2\pi h k_1 \lambda_1} \\ 0 \\ 0 \\ 0 \\ 0 \end{bmatrix}, \tag{16}$$

where the first row of matrix M is built using Eq. (13), while the second and third rows of matrix M are built using Eq. (14) and the fourth and fifth rows of matrix M are built using Eq. (15).

Solving the linear system defined in Eq. (16), the coefficients a_i and b_i in each region may be determined. Thereby, pressure change at the wellbore can be evaluated as:

$$\overline{G}_w(u) = a_1 I_0\left(r_w\sqrt{\frac{u}{\eta_1}}\right) + b_1 K_0\left(r_w\sqrt{\frac{u}{\eta_1}}\right). \tag{17}$$

Eq. (17) represents the pressure response measured at the wellbore due to the instant injection of a unitary volume of water into the reservoir at $t = 0$, as defined in the IBC given by Eq. (6). Thus, the term $\overline{G}_w$ denotes the impulse function (or Green's function) in Laplace domain (Carslaw and Jaeger, 1959, Gringarten and Ramey Jr., 1973), as a consequence of an instantaneous water injection of unitary volume. Note that the impulse function at the wellbore must be evaluated using the properties corresponding to Region 1, which is the region that contains the well. Thus, pressure change during an injectivity test may be determined as (Everdingen and Hurst, 1949, Prats et al., 2020):

$$\overline{\Delta p}_{wf}(u) = \overline{q_{inj}}(u)\overline{G}_w(u). \tag{18}$$

Finally, wellbore storage effects may be easily incorporated into Eq. (18) as follows (Everdingen and Hurst, 1949, Ehlig-Economides and Joseph, 1987, Spath et al., 1994):

$$\overline{\Delta p}_{wf}(u, C) = \frac{\overline{\Delta p}_{wf}(u, C = 0)}{1 + u^2 C \overline{\Delta p}_{wf}(u, C = 0)}, \tag{19}$$

where C stands for the storage coefficient.

In multilayer reservoirs, pressure change may be determined by combining Eq. (17) with the algorithm developed by Kuchuk and Wilkinson (1991).

Then, the following procedure may be applied to develop a computational implementation that computes the pressure change using the formulation detailed in this Section, for injectivity tests in multilayer reservoirs with vertical wells:

- Define an initial guess for layer flow-rates (*e.g.*, according to layer flow capacities)
- For each time step:
  1. For each layer:
     (a) Compute the water front radius, using Eq. (1)
     (b) Define each region of the radially composite reservoir model according to the water front position
     (c) Build matrix M
     (d) Evaluate the impulse function $\overline{G}_{w,j}(u)$, as defined in Eq. (17)
  2. Compute pressure change in Laplace domain $\overline{\Delta p}_{wf}$ as proposed by Kuchuk and Wilkinson (1991)
  3. Update layer flow-rates in Laplace domain $\overline{q}_j$ as proposed by Spath et al. (1994)
  4. Apply Stehfest (1970) algorithm to invert pressure change and flow-rates to the real time domain
- Repeat steps 1 to 4 for the next time step

2.2. Application to Single-Layer Reservoirs with Horizontal Wells

In reservoirs with horizontal wells, flow in each coordinate axis affects the pressure change behavior. The three-dimensional diffusivity equation for an isotropic reservoir is given by (Odeh and Babu, 1990, Larsen, 2000):

$$\frac{\partial^2 \Delta p}{\partial x^2} + \frac{\partial^2 \Delta p}{\partial y^2} + \frac{\partial^2 \Delta p}{\partial z^2} - \frac{1}{\eta}\frac{\partial \Delta p}{\partial t} = 0, \tag{20}$$

There already exist analytical models for single-phase flow in single-layer reservoirs with horizontal wells (Goode and Thambynayagam, 1987, Odeh and Babu, 1990, Daviau et al., 1988, Rosa and Carvalho, 1989). For a uniform influx wellbore, the solution in real time domain is obtained by applying Newman (1936) product and impulse functions (Gringarten and Ramey Jr., 1973, Ozkan et al., 1989, Kuchuk et al., 1991):

$$\Delta p(x, y, z, t) = q \int_0^t \Delta p_x(x, \tau)\Delta p_y(y, \tau)\Delta p_z(z, \tau) d\tau. \tag{21}$$

where Δp_x, Δp_y and Δp_z denote the respective impulse functions in x-, y- and z-directions.

When it comes to water injection in single-layer reservoirs with horizontal wells, an analytical model was developed by Peres and Reynolds (2003), based on the flooding patterns proposed by Deppe (1961). As explained by Peres and Reynolds (2003), the flood front initially propagates in the vertical plane perpendicular to the wellbore axis.

Therefore, this work proposes to approximate an injectivity test in a single-layer reservoir with horizontal well by a radially heterogeneous reservoir model. The reservoir is assumed to be isotropic ($k_x = k_y = k_z = k$). Fig. 7 shows a schematics of a single-layer reservoir with a horizontal injector well, for a given moment when the flood front is beyond the damaged region and assuming that the wellbore is parallel to the y-axis. Fig. 8 exhibits the view in zx-plane of this reservoir model.

As evidenced in Fig. 7, the approximated radially heterogeneous model for injectivity tests with horizontal wells considers that the flood front propagates only along the zx-plane. This assumption, albeit unrealistic, is expected to be reasonable, considering that the wellbore length is typically much longer compared to the reservoir thickness. Besides, water flow beyond the wellbore tips at early-times is also unaccounted for in the model proposed by Peres and Reynolds (2003).

One should notice, however, that waterfront propagation in the horizontal plane becomes increasingly more relevant as the injection goes on (Deppe, 1961, Peres and Reynolds, 2003, Peres et al., 2006, Bela et al., 2020b). Thus, the radially heterogeneous model exhibited in Figs. 7 and 8 is valid in an approximate sense, considering that the flood front has not yet reached a vertical boundary.

On the other hand, pressure transient front does not depend on the flood front position. Hence, considering the notation defined by Peres and Reynolds (2003), the approximate radially heterogeneous reservoir model shown in Figs. 7 and 8 is applicable for the "first radial - first radial", "first linear - first radial" and "second radial - first radial" flow-regimes.

Under those assumptions, and defining $r^2 = x^2 + z^2$, pressure change during injectivity tests in single-layer reservoirs with horizontal wells is governed by the following PDE:

$$\frac{\partial^2 \Delta p_i}{\partial y^2} + \frac{1}{r}\frac{\partial}{\partial r}\left(r\frac{\partial \Delta p_i}{\partial r}\right) - \frac{1}{\eta_i}\frac{\partial \Delta p_i}{\partial t} = 0. \quad (22)$$

Then, considering the impulse function defined in Section 2.1, this work proposes that pressure change at the wellbore in single-layer reservoirs with horizontal wells may be evaluated as:

$$\Delta p(y, r = r_w, t) = q \int_0^t \Delta p_y(y, \tau)\mathcal{L}^{-1}\left\{\overline{G}_w\right\}(\tau)d\tau, \quad (23)$$

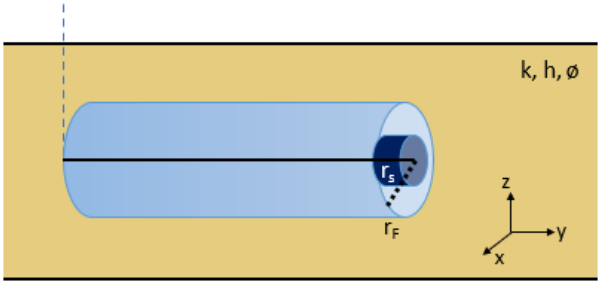

Figure 7: Horizontal injector well model (lateral view)

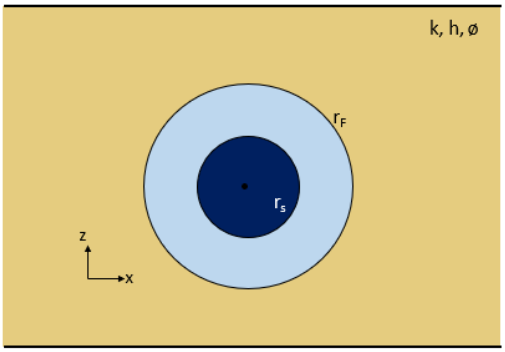

Figure 8: Horizontal injector well model (view of the zx-plane)

where $\overline{G}_w$ is the impulse function defined in Eq. (17) and $\Delta p_y(y,\tau)$ stands for the impulse function in y-direction, defined as (Daviau et al., 1988, Ozkan et al., 1989):

$$\Delta p_y(y,t) = \frac{1}{2}\left[\text{erf}\left(\frac{L-y}{2\sqrt{\eta t}}\right) - \text{erf}\left(\frac{-y}{2\sqrt{\eta t}}\right)\right], \tag{24}$$

where L indicates the wellbore length. The images method can be applied to depict the reservoir vertical boundaries (Clonts and Ramey Jr., 1986, Rosa and Carvalho, 1989).

Eq. (23) consists of an unorthodox application of Newman (1936) product, since it is derived from a non-homogeneous reservoir model, as shown in Figs. 7 and 8. A discussion regarding the accuracy of Eq. (23) is made in Section 3. A solid proof for why Eq. (23) would be an interesting topic for further research but is out of the scope of this work.

3. Results and Discussion

A comparison was made between a commercial flow simulator (CMG, 2010) and the formulations proposed in Section 2 in order to evaluate its accuracy on a set of synthetic cases. Additionally, the existing solutions for injectivity tests in multilayer reservoirs with vertical wells (Barreto Jr. et al., 2011, Mastbaum et al., 2021) and single-layer reservoirs with horizontal wells (Peres and Reynolds, 2003) were also compared to the models presented in Section 2.

In all cases, a piston-like fluid displacement was considered. The injection period was set as 96 h. Relative permeability data may be seen in Fig. 9.

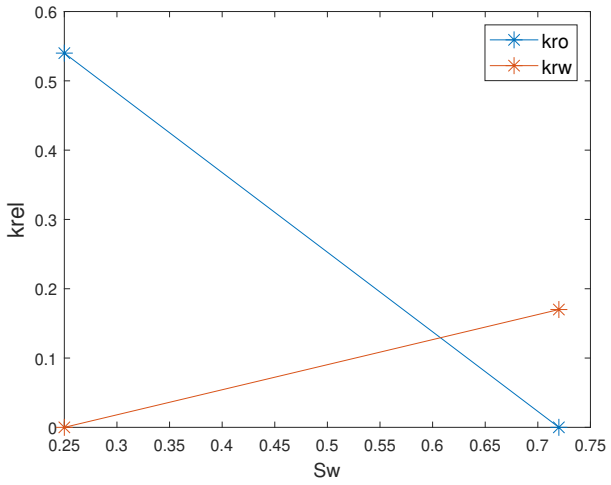

Figure 9: Relative permeability data

3.1. Results for Multilayer Reservoirs with Vertical Wells

The formulation proposed in Section 2.1 was implemented and compared to a commercial flow simulator (CMG, 2010). A cylindrical reservoir grid was employed, with 70 blocks in the radial direction and 1 block in the angular direction. In the vertical direction, each grid block represented a distinct layer. The reservoir outer radius was set as 4 km. The innermost grid block is 0.1 diameter wide and blocks get coarser as the distance to the wellbore increases.

The solutions developed by Barreto Jr. et al. (2011) and Mastbaum et al. (2021) for injectivity tests in multilayer reservoirs were also implemented and compared to the suggested model. Table 1 displays the reservoir properties for the multilayer cases. In all cases, a constant injection flow-rate

Case	μ_o (cP)	k (mD)	h (m)	ϕ	k_s (mD)	r_s (m)
A	4.8	500 600 700	15 20 25	0.11 0.25 0.33	200 (all)	0.4 (all)
B	1.1	500 600 700	15 20 25	0.11 0.25 0.33	200 (all)	0.4 (all)
C	4.8	500 700	20 15	0.11 0.25	200 (both)	0.4 (both)

Table 1: Reservoir properties for the multilayer cases

of 500 m^3/d was considered and wellbore storage effects were neglected.

Fig. 10 displays the loglog graphs of pressure and pressure derivative for Case A. Pressure data are represented in black and derivative curves are shown in blue. The formulation suggested in this work is indicated by circles. Triangles denote the numerical simulator. The dashed lines stand for the model proposed by Mastbaum et al. (2021) and the solid lines represent the solution developed by Barreto Jr. et al. (2011). The horizontal dashed line indicate the theoretical derivative level associated with oil properties, while the horizontal line in dash-dot pattern stands for the water properties theoretical derivative level.

A great agreement between all methods is observed. The sharp derivative drop that occurs at early times reflects the existence of skin effects (Peres and Reynolds, 2003, Bela et al., 2020a, Silva et al., 2021). Pressure derivative considering the numerical simulator data shows some divergence from the analytical solutions during this period. This may be related to the numerical grid discretization. Besides, the piston-like fluid displacement is more accurately depicted by the analytical models than the flow simulator. Still, after the damaged region is swept by water, all derivative curves converge.

It is also important to highlight that all methods attained the theoretical derivative level associated to the water properties. This indicates that the proposed formulation may be applied to estimate the reservoir equivalent permeability, based on the constant derivative level (Banerjee et al., 1998, Bela et al., 2019, 2020b). Fig. 10 also shows that the derivative curves attain values close to the oil derivative level at early-times but quickly detaches from this theoretical level, as the derivative drop starts.

Fig. 11 presents the layer flow-rate profiles for each methods, in semilog scale. The black curves denote layer 1, while blue curves stand for layer 2 and red curves represent layer 3. Fig. 11 evidences that layer flow-rates at the wellbore change in time. Hence, as mentioned in Section 1, it is unfeasible to assure that flow-rate within the swept zone remains constant in multilayer reservoirs. Layer 1 presents the lowest flow capacity, while layer 3 presents the highest flow capacity. Thereby, flow-rate in layer 1 is lower than in layer 2, which is lower than in

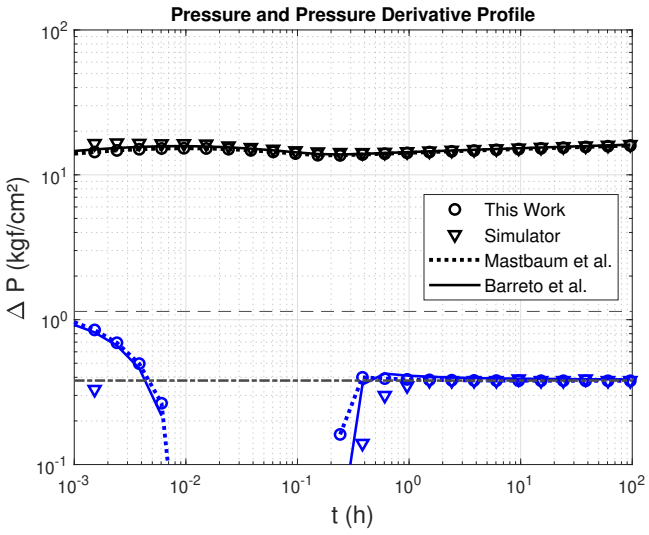

Figure 10: Pressure and derivative curves for case A

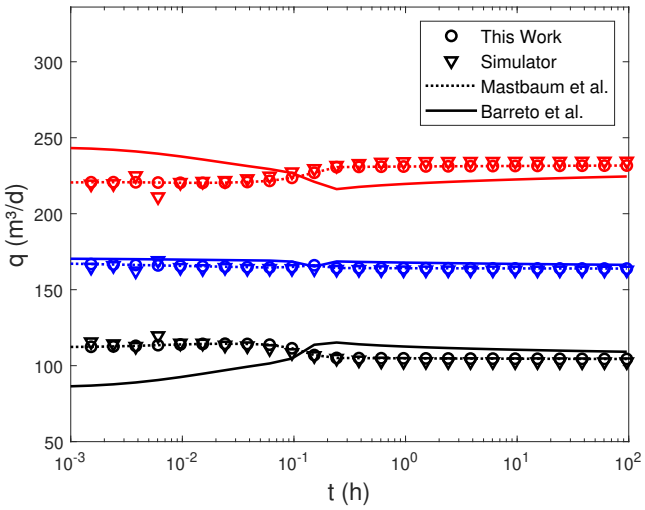

Figure 11: Layer flow-rate profiles for Case A (layer 1 in black; layer 2 in blue; layer 3 in red)

layer 3.

As disclosed in Fig. 11, the proposed formulation exhibits a close convergence to the simulated data and the analytical model from Mastbaum et al. (2021). However, flow-rate profiles computed using the analytical solution developed by Barreto Jr. et al. (2011) diverged from the other methods in layers 1 and 3. This result is particularly interesting, since accurate knowledge over layer flow-rate data is crucial for parameter estimation techniques (Coutinho et al., 2010, Guimarães and Galvão, 2017, Bela et al., 2020b).

Nonetheless, it is interesting to notice that the formulation proposed by Barreto Jr. et al. (2011) was able to provide pressure and pressure derivative curves that accurately match the other methods, despite the divergence observed in the layer flow-rate profiles.

Pressure and derivative curves for case B may be seen in Fig. 12. Case B presents the same reservoir properties as Case A, expect for oil viscosity. Therefore, the theoretical oil derivative level is now lower than the water derivative level. The hump in pressure derivative curves that occurs between $t \approx 0.01$ h and $t \approx 0.2$ h reflects the existence of skin effects in reservoirs where flow is favorable to oil (Bela et al., 2020a, Silva et al., 2021). After this derivative hump, flood front propagates throughout the undamaged zone.

Similarly to Case A, all methods presented a close agreement. The three analytical formulations converged during the entire test, while numerical data presented some slight divergences at early times, when the flood front is still within the damaged zone. Despite that, the overall agreement is quite good and all methods converged towards the theoretical water derivative level, indicating that late-time data can be used to determine the reservoir equivalent permeability.

Layer flow-rates for Case B are reported in Fig. 13. The formulation suggested in Section 2 exhibits an excellent agreement with the solution developed by Mastbaum et al. (2021). Flow-rates evaluated using these analytical models show a similar behavior to the numerical simulator flow-rate curves. Yet, in layers 1 and 3, the match between analytical and simulated data is not as close as observed in Case A.

On the other hand, flow-rate profiles determined by the solution proposed by Barreto Jr. et al. (2011) presented once again noticeable differences

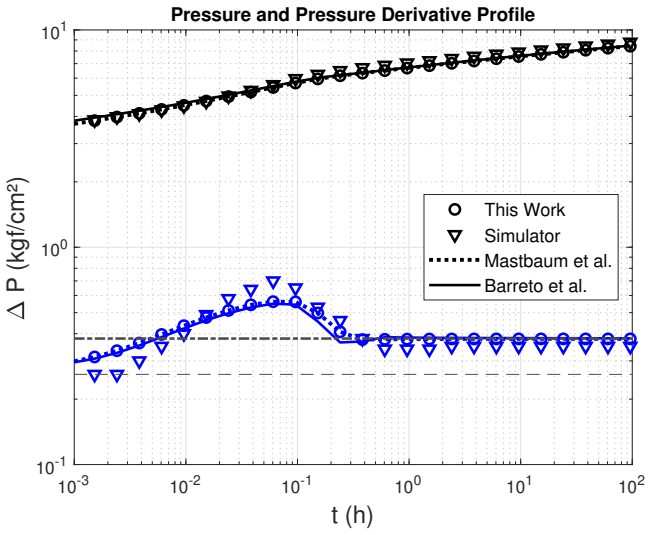

Figure 12: Pressure and derivative curves for case B

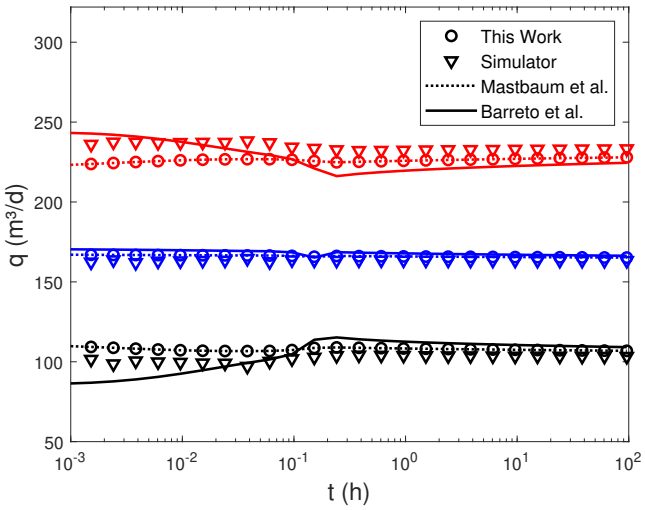

Figure 13: Layer flow-rate profiles for Case B (layer 1 in black; layer 2 in blue; layer 3 in red)

compared to the other methods. Figs. 12 and 13 show that the solution from Barreto Jr. et al. (2011) provided a good match for pressure data but yielded layer flow-rate profiles that diverged from the other models, as occurred in Case A.

Pressure and derivative data for Case C may be observed in Fig. 14. The overall behavior is similar to Case A: pressure change presented a close agreement for all methods, as well as the derivative curves. The blunt derivative drop at early-times indicates the existence of formation damage. At late-times, the theoretical derivative level associated with water properties is attained by all models.

In Case C, layer flow-rate curves, portrayed in Fig. 15, provide a more interesting analysis than pressure and derivative data. Fig. 15 evidence that both the formulation proposed in Section 2.1 and the solution presented by Mastbaum et al. (2021) exhibited a great agreement with the numerical data. As mentioned earlier, accurate evaluation of flow-rates in each layer is helpful to some interpretation techniques that aim to estimate individual layer properties (Ehlig-Economides and Joseph, 1987, Coutinho et al., 2010, Galvão and Guimarães, 2017, Bela et al., 2020b).

Similar to the previous cases, flow-rates computed using the solution from Barreto Jr. et al. (2011) diverged from the other analytical models and from the numerical simulator. Moreover, the solution from Barreto Jr. et al. (2011) presented the most significant variations in layer flow-rates, even though this is the only analytical model that requires flow-rate to be constant within the swept region. Despite that, it is interesting to notice the close agreement presented by the pressure and derivative curves in Fig. 14.

Pressure and layer flow-rate profiles displayed in Figs. 10 to 15 were employed to estimate layer permeabilities using the Delta Transient Method (Galvão and Guimarães, 2017, Guimarães and Galvão, 2017). This procedure requires pressure and flow-rate data from only two distinct time steps, which is a significant operational advantage (Bela et al., 2020b).

In this work, the late-time logarithmic approximation based on water properties was employed to evaluate layer permeabilities. For all methods, pressure and flow-rate data at $t = 6.06$ h and $t = 60.6$ h were used to evaluate layer permeabil-

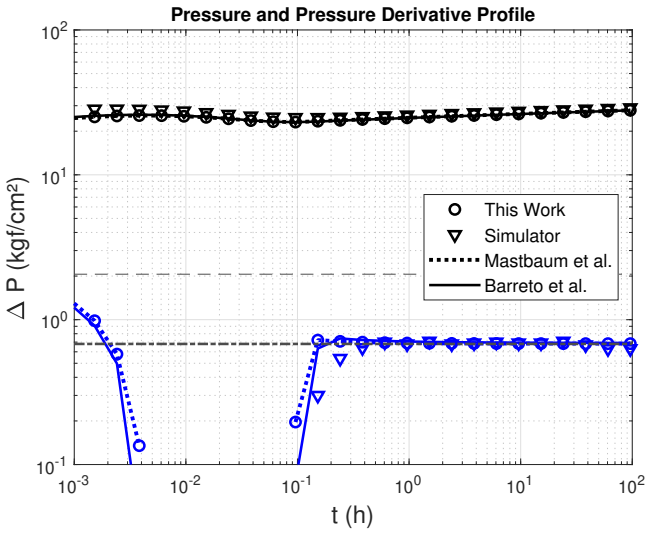

Figure 14: Pressure and derivative curves for case C

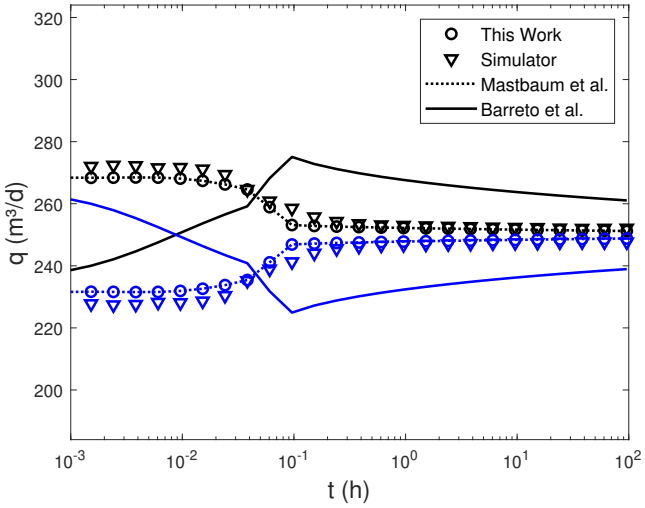

Figure 15: Layer flow-rate profiles for case C (layer 1 in black; layer 2 in blue)

		This Work		Num. Simulator		Mastbaum et al.		Barreto et al.	
Case	True	Est.	Er. (%)	Est.	Er. (%)	Est.	Er. (%)	Est.	Er. (%)
A	500	498	-0.3	493	-1.4	498	-0.3	429	-14.2
	600	599	-0.2	589	-1.8	599	-0.2	560	-6.7
	700	700	0.0	691	-1.3	700	0.0	767	9.6
B	500	501	0.1	500	0.1	501	0.1	481	-3.7
	600	600	0.1	599	-0.2	600	0.1	590	-1.6
	700	700	-0.1	700	0.0	700	-0.1	716	2.2
C	500	499	0.2	497	-0.7	499	-0.2	448	-10.4
	700	701	0.1	683	-2.4	701	0.1	804	14.8

Table 2: Estimated Layer Permeabilities (Values in mD)

ities. Figs. 10, 12 and 14 evidence that, for all cases, a radial flow regime occurs during this time range, since derivative remains constant.

Table 2 displays the estimated layer permeabilities considering each approach employed to compute the pressure change. A great accuracy may be observed in all cases. Moreover, the formulation presented in this work yielded values very close to the estimates obtained from the flow simulator and the model proposed by Mastbaum et al. (2021). The solution developed by Barreto Jr. et al. (2011), in its turn, showed some differences compared to the other models (particularly in case B), despite presenting a decent accuracy.

These divergences are likely related to the mismatch between layer flow-rate data. As displayed in Figs. 11, 13 and 15, flow-rates evaluated using the solution developed by Barreto Jr. et al. (2011) diverged from the other approaches, which yielded similar flow-rate profiles. These results combined with the higher errors in layer permeabilities observed in Table 2 suggest that layer flow-rate profiles computed using their model are less accurate than the flow-rate curves obtained from the other methods.

3.2. Results for Single-Layer Reservoirs with Horizontal Wells

A computational implementation of the analytical model presented in Section 2.2 was developed and compared to the solution proposed by Peres and Reynolds (2003) for injectivity tests in single-layer reservoirs with horizontal wells. Results were also compared to the commercial flow simulator (CMG, 2010).

A cartesian grid composed of 61 x 61 x 9 blocks was employed. Again, blocks closer to the wellbore were more refined than blocks further from it. Reservoir grid was 6,000 m wide (x-direction) and 6,300 m long (y-direction). The wellbore was built parallel to the y-direction. Length (y-direction) of each block containing the wellbore was set as 100 m, while width (x-direction) and height (z-direction) were set as 0.89 m. Therefore, the skin zone radius was set as 0.5 m in the analytical models, so that the damaged region presents the same cross-sectional area that the numerical simulation grid. A hybrid refinement of 4 (radial direction) by 4 (angular direction) by 4 (well axis direction) was employed at all grid blocks containing the wellbore.

The numerical simulator considers an infinite conductivity wellbore, while both analytical solutions assume uniform influx. Either the average pressure technique (Kuchuk et al., 1991, Kuchuk and Habashy, 1996, Chen et al., 1991) or the equivalent pressure point (Ozkan et al., 1989, Daviau et al., 1988, Rosa and Carvalho, 1989, Jelmert and Thompson, 1991) may be applied to obtain the pressure change at an infinite conductivity wellbore using a formulation that assumes uniform in-

Case	μ_o (cP)	k (mD)	h (m)	L (m)	ϕ	k_s (mD)	r_s (m)
D	4.8	2000	25	700	0.25	500	0.5
E	1.1	2000	25	700	0.25	500	0.5

Table 3: Reservoir properties for cases with horizontal well

flux. While the average pressure technique may be more accurate, its implementation is also more complex. For this reason, the equivalent pressure point was employed to obtain the pressure change corresponding to an infinite conductivity wellbore. Thus, pressure change in the analytical formulations was evaluated at $x = z = r_w$ and $y = 0.732$ times the wellbore length, as suggested by Ozkan et al. (1989).

Layer properties for the tested cases may be found in Table 3. Injection flow-rate was defined as 5,000 m^3/d for Cases D and E. As in Section 3.1, wellbore storage effects were disregarded. Reservoir properties are the same in both cases, except for the oil viscosity. The horizontal well was assumed to be at the center of the layer; that is, no off-centering was considered. Waterfront radius at the end of the 96h injection period, determined by Eq. (1), was equal to 8.8 m. Thus, the flood front has not yet reached the reservoir vertical boundaries and the formulation developed in Section 2.2 is applicable.

Fig. 16 displays the pressure and pressure derivative data for Case D. Black curves denote the pressure data while the blue curves correspond to the derivative profile. The model proposed in Section 2.2 is indicated by circles. Triangles represent the numerical simulator and the solid lines correspond to the solution presented by Peres and Reynolds (2003). The horizontal dashed line indicates the theoretical pressure derivative profile for "first radial - first radial" flow regime, as defined by Peres and Reynolds (2003). At late-times, the flood front is still propagating in the vertical plane, while pressure diffusion is occurring in the horizontal direction. Therefore, a "second radial

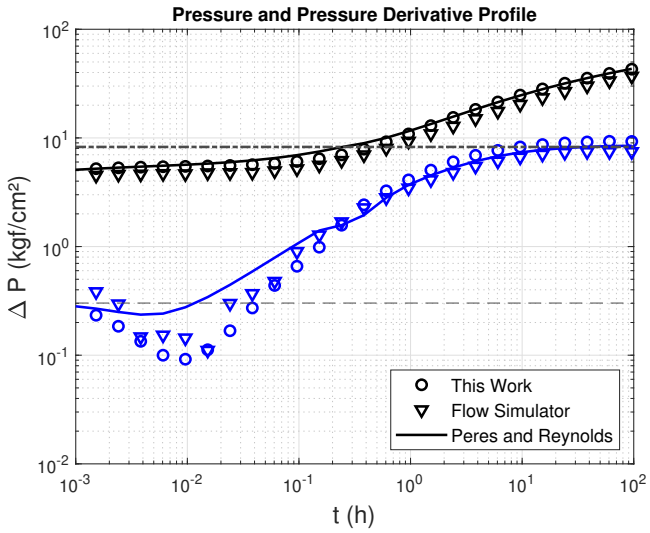

Figure 16: Pressure and derivative curves for case D

- first radial" occurs at the end of the test. The dash-dotted horizontal line stands for the theoretical level for this flow regime.

A good agreement is observed between all curves. As in Section 3.1, the pressure derivative drop observed at early-times indicates the existence of formation damage. Pressure derivative for the numerical simulator presents some oscillations for short times ($t \leq 3 \cdot 10^{-2}$ h). These oscillations are possibly explained by the grid discretization and how the numerical simulator accuracy to represent a piston-like flow. Despite that, numerical data match well the analytical models.

It is worthy to mention that, interestingly enough, the proposed formulation based on an unusual application of Newman (1936) product presents a closer match to the simulator derivative curve than the solution developed by Peres and Reynolds (2003) at early-times. Furthermore, all methods attain the late-time theoretical derivative level.

The results for Case E may be seen in Fig. 17. All methods exhibit a great match not only for pressure but also for derivative data. In Case E, the derivative curves quickly detach from the early-time theoretical level. Still, the derivative signa-

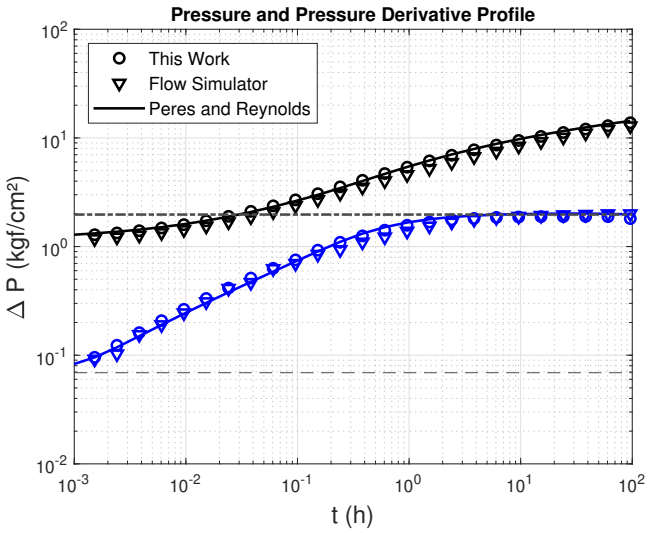

Figure 17: Pressure and derivative curves for case E

ture that indicates a late-time radial flow is clearly observed. This constant derivative level is useful to determine the reservoir permeability (Odeh and Babu, 1990, Rosa and Carvalho, 1989, Boughara and Reynolds, 2009).

Since Case E presents a mobility ratio lower than unity, no derivative drop is observed. One could expect a derivative hump instead, similar to cases B and C. However, this hump may be masked by the derivative rise due to the linear flow regime. Yet, it is interesting to notice once again the close agreement presented by the proposed solution, considering the application of Newman (1936) product for a non-homogeneous reservoir model.

4. Summary and Conclusions

This work presents an alternative solution for injectivity tests in single-layer reservoirs. The suggested formulation uses a radially composite reservoir model with moving boundary to depict the swept region (Bratvold and Horne, 1990, Neto et al., 2020, Mastbaum et al., 2021, Viana, 2021) and applies impulse functions to obtain the pressure change at the wellbore. The single-layer solution may be coupled to the algorithm developed by Kuchuk and Wilkinson (1991) to evaluate the pressure behavior in multilayer reservoirs. A formulation is also proposed for injectivity tests in single-layer reservoirs with horizontal wells by combining the proposed single-layer solution to an unusual application of Newman (1936) product.

The suggested formulations were compared to a commercial flow simulator (CMG, 2010) and to previously existing solutions (Peres and Reynolds, 2003, Barreto Jr. et al., 2011, Mastbaum et al., 2021). Results for the multilayer cases (seen in Section 3.1) showed that the proposed model fits well the pressure and flow-rate data provided by the numerical simulator.

Furthermore, results evidence that layer-flow rates do not remain constant in time. This is a relevant outcome, as it demonstrates that, rigorously speaking, the Thompson and Reynolds (1997) steady-state theory does not hold for multilayer reservoirs. Despite that, it is interesting to notice that all methods presented a good match for pressure and pressure derivative data. On the other hand, layer flow-rate curves computed by the solution developed by Barreto Jr. et al. (2011) presented significant divergences compared to the analytical model proposed in this work, to the other models.

The Delta Transient Method (Galvão and Guimarães, 2017) was employed to estimate individual layer permeabilities. Results showed a satisfactory accuracy. Furthermore, estimates obtained from all models except the model presented by Barreto Jr. et al. (2011) were very close to each other. This outcome and the aforementioned divergences in layer flow-rate curves suggest that the formulation developed by Barreto Jr. et al. (2011) is less accurate to evaluate flow-rate behavior than the other approaches, despite yielding a decent match for pressure and derivative data.

Results from Section 3.2 verify that the unorthodox application of Newman (1936) product suggested in Section 2.2 was able to provide a formulation for injectivity tests in single-layer reservoirs

with horizontal wells that matches well the results from a commercial flow simulator and also the solution developed by Peres and Reynolds (2003). A solid proof to justify the application of Newman (1936) product using a radially heterogeneous reservoir model was out of the scope of this work, and remains as suggestion for further research.

Nomenclature

a = Multiplicative coefficient, defined in Eq. (11)
b = Multiplicative coefficient, defined in Eq. (11)
C = Wellbore storage coefficient [m^3/Pa, STB/psi, m^3/(kgf/cm^2)]
c = Compressibility, [$(Pa)^{-1}$, $(kgf/cm^2)^{-1}$]
erf = Error function
f'_w = Fractional flow derivative [–]
G_w = Impulse function in Laplace domain
h = Thickness [m, ft]
I_i = Modified Bessel function of first kind and order i
K_i = Modified Bessel function of second kind and order i
k = Permeability [m^2, mD]
k_r = Relative permeability [–]
L = Wellbore length [m, ft]
M = Matrix defined in Eq. (16)
p = Pressure [Pa, psia, kgf/cm^2]
q = Flow-rate [m^3/s, STB/d, m^3/d]
r = Radius [m, ft]
r_w = Wellbore radius [m, in]
S_w = Water saturation [–]
t = Time [s, h]
u = Laplace variable
δ = Dirac delta function
η = Hydraulic diffusivity coefficient [m^2/s, mD·psia/cP, mD· kgf/cm^2/cP]
λ = Fluid mobility $[(Pa{\cdot}s)^{-1}, (cP)^{-1}]$
ϕ = Porosity [–]
τ = Silent time integration variable [s, h]

Subscripts

F = Related to the flood front
i = Related to region i
inj = Related to the injected fluid
j = Related to layer j
o = Related to oil
s = Related to the damaged region
t = Total
x = With respect to x-direction
y = With respect to y-direction
z = With respect to z-direction

Acknowledgements

Authors are grateful to Petrobras for partially sponsoring this research as part of project TCBR 485. This study was financed in part by the Coordenação de Aperfeiçoamento de Pessoal de Nível Superior - Brasil (CAPES) - Finance Code 001. The first author also thanks D.Sc. Thiago M. D. Silva due to his comments that helped to improve this manuscript. This work is theoretical and does not contain any real field data.

References

Abramowitz, M. and Stegun, I. A. (1964). *Handbook of Mathematical Functions*. Number 55 in Applied Mathematics Series. United States National Bureau of Standards, Washington, DC.

Ahmed, T. (2010). *Reservoir Engineering Handbook*. Elsevier, Oxford, UK.

Banerjee, R., Thompson, L. G., and Reynolds, A. C. (1998). Injection/falloff testing in heterogeneous reservoirs. *SPE Reservoir Evaluation & Engineering*, December:519–527.

Barreto Jr., A. B., Peres, A. M. M., and Pires, A. P. (2011). Water injectivity tests on multilayered oil reservoirs. *Paper presented at the Brasil Offshore Conference and Exhibition*, June:1–11.

Bela, R. V., Pesco, S., and Barreto Jr., A. B. (2019). Modeling falloff tests in multilayer reservoirs. *Journal of Petroleum Science and Engineering*, 174:161–168.

Bela, R. V., Pesco, S., and Barreto Jr., A. B. (2020a). Determining skin zone properties from injectivity tests in single and multilayer reservoirs. *Journal of Petroleum Exploration and Production Technology*, 10:1459–1471.

Bela, R. V., Pesco, S., Barreto Jr., A. B., and Onur, M. (2020b). Analytical solutions for injectivity and falloff tests in stratified reservoirs with multilateral horizontal wells. *Journal of Petroleum Science and Engineering*, 197.

Bela, R. V., Pesco, S., Barreto Jr., A. B., and Onur, M. (2022). Assisted history matching and graphical methods for estimating individual layer properties from well testing data in stratified reservoirs with multilateral wells. *Journal of Petroleum Science and Engineering*, 208, part A.

Bonafé, M. F., Braga, A., and Barreto Jr., A. B. (2020). Approximate solution for pressure during a multiple rate injectivity test. *Journal of Petroleum Exploration and Production Technology*, 10:2373–2386.

Borello, E. S., Fokker, P. A., Viberti, D., Verga, F., Hofmann, H., Meier, P., Min, K.-B., Yoon, K., and Zimmermann, G. (2019). Harmonic pulse testing for well monitoring: Application to a fractured geothermal reservoir. *Water Resources Research*, 55:4727–4744.

Boughara, A. A. and Reynolds, A. C. (2009). Analysis of injection/falloff data from horizontal wells. *SPE Journal*, December:721–736.

Bratvold, R. B. and Horne, R. N. (1990). Analysis of pressure-falloff tests following cold-water injection. *SPE Formation Evaluation*, September:293–302.

Buckley, S. E. and Leverett, M. C. (1942). Mechanism of fluid displacement in sands. *Transactions of the AIME*, 146:107–116.

Carslaw, H. S. and Jaeger, J. C. (1959). *Conduction of Heat in Solids*. Second Edition. Oxford University Press, London, U.K.

Chen, H.-Y., Raghavan, R., and Poston, S. W. (1991). An application of the product-solution principle for instantaneous source and green's functions. *SPE Formation Evaluation*, June:161–168.

Clonts, M. D. and Ramey Jr., H. J. (1986). Pressure-transient analysis for wells with horizontal drainholes. *paper presented at SPE California Regional Meeting*, April:215–230.

CMG (2010). *IMEX User Guide*. Computer Modeling Group, Calgary, Alberta, Canada.

Coutinho, E. J. R., Emerick, A. A., Li, G., and Reynolds, A. C. (2010). Conditioning multilayered geologic models to well-test and production-logging data using the ensemble kalman filter. *paper presented at SPE Annual Technical Conference and Exhibition*, September:1–19.

Daviau, F., Mouronvai, G., Bourdarot, G., and Curutchet, P. (1988). Pressure analysis for horizontal wells. *SPE Formation Evaluation*, December:716–724.

Deppe, J. C. (1961). Injection rates - the effect of mobility ratio, area swept and pattern. *SPE Journal*, June:81–91.

Ehlig-Economides, C. A. and Joseph, J. (1987). A new test for determination of individual layer properties in a multilayered reservoir. *SPE Evaluation Formation*, September:261–283.

Equinor (2021). Our climate ambitions - net zero by 2050 (accessed in july, 2021). `www.equinor.com/en/sustainability/climate.html`.

Everdingen, A. F. V. and Hurst, W. (1949). The application of the laplace transformation to flow problems in reservoirs. *Petroleum Transactions*, December:305–324.

Galvão, M. S. C. and Guimarães, C. S. (2017). A new method for calculating individual layer permeability and skin in a multilayered reservoir using production logging data: The delta transient method. *Paper presented at the SPE Latin America and Caribbean Mature Fields Symposium*, March:1–30.

Gao, C.-T. (1987). Determination of parameters for individual layers in multilayer reservoirs by transient well tests. *SPE Formation Evaluation*, March:43–65.

Goode, P. A. and Thambynayagam, R. K. M. (1987). Pressure drawdown and buildup analysis of horizontal wells in anisotropic media. *SPE Formation Evaluation*, December:683–697.

Gringarten, A. C. and Ramey Jr., H. J. (1973). The use of source and green's functions in solving unsteady-flow problems in reservoirs. *SPE Journal*, October:285–296.

Guimarães, C. S. and Galvão, M. S. C. (2017). Application of the delta transient method to multi-rate tests: A method for calculating individual layer permeability and skin in a multilayered reservoir using production logging data. *Paper presented at the Offshore Technology Conference Brasil*, pages 1–22.

Jelmert, T. A. and Thompson, L. G. (1991). Horizontal wells - a test on infinite conductivity solutions. *Paper presented at SPE International Arctic Technology Conference*, May:1–20.

Kuchuk, F. J., Goode, P. A., Wilskinson, D. J., and Thambynayagam, R. K. M. (1991). Pressure-transient behavior for horizontal wells with and without gas cap or aquifer. *SPE Formation Evaluation*, March:86–94.

Kuchuk, F. J. and Habashy, T. (1996). Pressure behavior of horizontal wells in multilayer reservoirs with crossflow. *SPE Formation Evaluation*, March:55–64.

Kuchuk, F. J. and Wilkinson, D. J. (1991). Transient pressure behavior of commingled reservoirs. *SPE Formation Evaluation*, March:111–120.

Larsen, L. (2000). Pressure-transient behavior of multibranched wells in layered reservoirs. *SPE Reservoir Evaluation & Engineering*, February:68–73.

Lefkovits, H. C., Hazebroek, P., Allen, E. E., and Matthews,

C. S. (1961). A study of the behavior of bounded reservoirs composed of stratified layers. *SPE Journal*, March:43–58.

Lu, J., Zhou, B., Rahman, M. M., and He, X. (2019). New solution to the pressure transient equation in a two-layer reservoir with crossflow. *Journal of Computational and Applied Mathematics*, 362:680–693.

Lukoil (2021). Reduced greenhouse gas emissions (accessed in august, 2021). `www.lukoil.com/Sustainability/Climatechange/GHGEmissions`.

Mastbaum, A. L., de Souza, A. B., Neto, J. L. F. B., Bela, R. V., and Barreto Jr., A. B. (2021). Dual-phase flow in multilayered porous media - a radial composite laplace domain approximation. *Journal of Petroleum Exploration and Production Technology*.

Neto, A. d. C. L. (2019). Modelagem matemática de testes de pressão em reservatórios de gás com região de permeabilidade reduzida em torno dos poços. Ms thesis, Universidade Estadual do Norte Fluminense (UENF).

Neto, J. L. F. B., Bela, R. V., Pesco, S., and Barreto Jr., A. B. (2020). Pressure behavior during injectivity tests - a composite reservoir approach. *Paper presented at the SPE Latin American and Caribbean Petroleum Engineering Conference*, July:1–18.

Newman, A. B. (1936). Heating and cooling rectangular and cylindrical solids. *Industrial and Engineering Chemistry*, 28:545–548.

Nie, R.-S., Guo, J.-C., Jia, Y.-L., Zhu, S.-Q., Rao, Z., and Zhang, C.-G. (2011). New modelling of transient well test and rate decline analysis for a horizontal well in a multiple-zone reservoir. *Jornal of Geophysiscs and Engineering*, 8:464–476.

Occidental (2021). Climate report 2020 (accessed in august, 2021). `www.oxy.com/Sustainability/overview/Documents/ClimateReport2020.pdf`.

Odeh, A. S. and Babu, D. K. (1990). Transient flow behavior of horizontal wells, pressure drawdown and buildup analysis. *SPE Formation Evaluation*, March:7–15.

Ozkan, E., Raghavan, R., and Joshi, S. D. (1989). Horizontal well pressure analysis. *SPE Formation Evaluation*, December:567–575.

Peres, A. M. M., Boughara, A. A., and Reynolds, A. C. (2006). Rate superposition for generating pressure falloff solutions. *SPE Journal*, September:364–374.

Peres, A. M. M. and Reynolds, A. C. (2003). Theory and analysis of injectivity tests on horizontal wells. *SPE Journal*, June:147–159.

Petrobras (2021). Relatório de sustentabilidade 2020 (in portuguese, accessed in august, 2021). `sustentabilidade.petrobras.com.br`.

Petronas (2021). Net zero carbon emissions (accessed in august, 2021). `www.petronas.com/sustainability/net-zero-carbon-emissions`.

Prats, M., Meneses-P., L. L., Samaneigo-V., F., and Pacheco-V., R. (2020). Pressure buildup in a well produced at constant pressure. *SPE Journal*, 25:1578–1598.

Raghavan, R. (1989). Behavior of wells completed in multiple producing zones. *SPE Evaluation Formation*, June:219–230.

Rosa, A. J. and Carvalho, R. d. S. (1989). A mathematical model for pressure evaluation in an infinite-conductivity horizontal well. *SPE Formation Evaluation*, December:559–566.

Shell (2021). Our climate target (accessed in july, 2021). `www.shell.com/energy-and-innovation/the-energy-future/our-climate-target.html#iframe=L3dlYmFwcHMvY2xpbWF0ZV9hbWJpdGlvbi8`.

Silva, T. d. M. D., Bela, R. V., Pesco, S., and Barreto Jr., A. B. (2021). Es-mda applied to estimate skin zone properties from injectivity tests data in multilayer reservoirs. *Computers & Geosciences*, 146:1–18.

Spath, J. B., Ozkan, E., and Raghavan, R. (1994). An efficient algorithm for computation of well responses in commingled reservoirs. *SPE Formation Evaluation*, June:115–121.

Stehfest, H. (1970). Algorithm 368: Numerical inversion of laplace transforms [d5]. *Communications of the ACM*, 13:47–49.

Thompson, L. G. and Reynolds, A. C. (1997). Well testing for radially heterogeneous reservoirs under single and multiphase flow conditions. *SPE Evaluation Formation*, March:57–64.

Viana, I. V. (2021). An analytical model for injectivity tests in multilayered reservoirs with formation crossflow. Ms thesis, Pontifícia Universidade Católica do Rio de Janeiro (PUC-Rio).